

A Wide Depth Distribution of Seismic Tremors Along the Northern Cascadia Margin

Honn Kao, Shao-Ju Shan, Herb Dragert, Garry Rogers, John F. Cassidy, & Kumar Ramachandran

Geological Survey of Canada, Pacific Geoscience Centre, 9860 West Saanich Road, Sidney, British Columbia V8L 1B9, Canada

The Cascadia subduction zone is capable of generating major earthquakes with moment magnitude as large as 9 at an interval of several hundred years¹⁻³. The seismogenic portion of the plate interface is mostly offshore and currently locked as inferred from geodetic data⁴⁻⁶. However, episodic surface displacements in the direction opposite to the long-term deformation motions caused by relative plate convergence across a locked interface are observed about every 14 months with a unique tremor-like seismic signature⁷⁻⁹. Here we show that these tremors are distributed over a depth range exceeding 40 km within a limited horizontal band. Many occurred within or close to the strong seismic reflectors above the plate interface where local earthquakes are absent, suggesting that the seismogenic process for tremors is fluid-related. The observed depth range implies that tremors could be associated with the variation of stress field induced by a transient slip along the deeper portion of the Cascadia interface or, alternatively, episodic slip is more diffuse than originally suggested.

In anticipation of an episodic tremor-and-slip (ETS) event⁷⁻⁹ in February–March 2003, the Geological Survey of Canada augmented the existing seismographic network by deploying temporary broad band instruments to create a dense seismic array in southern Vancouver Island (Figure 1). Clear tremor signals were first observed on February 25, 2003 (defined as Day 0) and lasted for more than 3 weeks (Figure 1).

Concurrently, the GPS site near Victoria, at the southern tip of Vancouver Island, showed a steady westward movement during the first 10 days with a total displacement of ~ 3.7 mm. The GPS site located ~ 175 km toward the northwest near Ucluelet, however, showed little or no corresponding movement, implying that the slip was mostly beneath the southern Vancouver Island.

Because of the emergent arrivals and the clustering nature of tremor signals, determination of tremor origin times and locations using standard seismological procedures becomes extremely difficult. The newly developed Source-Scanning Algorithm (SSA) method is used instead to overcome such problems¹⁰. The SSA method identifies the existence of seismic sources in space and time by calculating the so-called “brightness” function for all grid points inside the model space. The larger value of the brightness function means a better consistency between the identified sources (i.e., epicenter, depth, and origin time) and observed waveforms. A more detailed description of our SSA analysis and a list of determined tremor locations and origin times are presented as an online supplement to this article.

The most striking result of our analysis is that ETS tremors are distributed across a wide depth range of over 40 km, with a peak at the depth of 25–35 km. Two representative examples, one centered at a shallow depth of 11 km and another at 48 km, are shown in Figure 2 to demonstrate that this wide span cannot be attributed to analysis uncertainties (which are estimated to be ± 3 and ± 5 km for epicentral location and depth, respectively). Forward calculations indicate that there is virtually no trade-off between the determined depth and origin time because of the optimal station coverage (Figures 1 and 2). We also conducted a series of experiments to confirm that the depth difference did not arise from a systematic bias in the velocity model and/or different choices of controlling parameters used in the SSA analysis (see the online supplement for details). For a few relatively large and isolated tremors, the best

solutions are further verified by conventional earthquake location methods and/or 3-D relocation techniques. All results consistently suggest the existence of ETS tremors over a wide depth range.

The epicenters of most tremors are confined to a limited band bounded approximately by the surface projections of 30- and 45-km depth contours of the subducting plate interface, with a clear northwestward migration pattern (Figure 1). We construct two cross sections to show the depth distribution of ETS tremors in Figure 3. The southern section (A–B) corresponds to the initial stage of this ETS sequence (Days 0–6), whereas the northern section (C–D) represents the ending phase. Background seismicity since 1990 is also plotted for comparison. It is clear that ETS tremors do not occur strictly along the plate interface (or any other planar structures) as has been proposed for the slip⁷. Instead, they are distributed in both the overriding crust and within the subducted slab (as demonstrated by examples in Figure 2), similar to the pattern of local earthquakes (Figure 3).

However, ETS tremors have the tendency to occur in places where local earthquakes are sparse. This is confirmed by simple “nearness” tests on both the tremor and earthquake datasets. On average, the distance from one tremor to the nearest earthquake hypocenter is ~10 km, about double of that to the nearest tremor (~5 km). In contrast, the average earthquake-to-earthquake “nearness” is only 3 km, suggesting that the difference between the spatial distributions of tremors and earthquakes is not an artifact.

This difference becomes more apparent when the cross sections are overlaid with available tomographic images¹¹ and seismic reflection profiles (Figure 3). While 50–55% of ETS tremors are located within or close to the strong reflectors above the plate interface, >90% of local earthquakes tend to locate away from the reflectors^{12,13}.

Previous studies have shown that these strong reflectors coincide with an electrically conductive layer¹⁴⁻¹⁶ and a low shear wave velocity zone¹⁷. It has been argued that these regions are where fluids released from the dehydration reactions in the subducted oceanic slab are trapped¹³⁻¹⁶. Theoretical calculations of the amplitude contrast also suggest that the reflectors may be associated with extensive shearing¹³⁻¹⁵. Consequently, the observed tremor distribution suggests that the underlying physical processes, which might be closely related to both shear deformation and fluids, are distinct from those involved in earthquake rupture.

Another noticeable difference can be found in the frequency contents of ETS tremors and local earthquakes (Figure 4). To ensure that the calculated frequency spectra are representative of the source characteristics with minimum path effects, we only include seismograms recorded within 50 km from the corresponding earthquake or tremor epicenters. The two tremor datasets contain seismograms corresponding to the 10 largest tremors observed in this ETS sequence and the 10 best located tremors in this study, respectively, whereas the three earthquake datasets are for different magnitude ranges (M_L 2.5–3.5, 1.0–1.5, and 0.0–0.2). It is obvious that the stacked Fourier spectra of ETS tremors show relatively larger amplitudes in the frequency range of 1–5 Hz with a rapid decrease at higher (5–30 Hz) frequencies (Figure 4). The sharp contrast in the frequency characteristics between ETS tremors and earthquakes again hints at different seismogenic behavior.

Our results provide important insights into the physical/mechanical processes along the Cascadia margin that subsequently control the seismogenic/rheological behavior of the subduction system. If fluid released from dehydration of subducted materials plays an important role in forming the strong seismic reflectors in Cascadia's forearc as suggested previously^{14,15,18}, it may also play a critical role in facilitating the occurrence of ETS tremors. One possible scenario is that ETS tremors manifest the

hydro-seismic processes in both the overriding continental crust and the subducting oceanic crust in response to the temporal stress/strain field induced by the transient slip along the deeper (aseismic) portion of the plate interface. In this case, the existence of fluids provides a favorable condition for tremors to occur, whereas the stress/strain variation due to the transient slip actually triggers their occurrences. Alternatively, if the tremors are interpreted as the de facto seismic part of the episodic slip, then the slip may have occurred in a zone much more diffuse than previous studies have suggested⁷.

While the inversion of surface GPS measurements cannot rule out the latter scenario, it is not only more complex but could also introduce a mass balance problem in the forearc region, if the diffused slip above the plate interface continues over geological time scales and permanently displaces material through shearing¹⁹. However, many other processes can be involved in the mass balance issue in the forearc region, including frontal accretion that transfers materials into the wedge²⁰, subduction erosion or underplating at the base of the forearc²¹, and regional N–S crustal shortening²². From our observations alone, we cannot conclusively reject either interpretation at this stage.

Whichever interpretation is chosen, a concurrence of tremors and slip in an ETS event is always implied. However, the original ETS report acknowledged the existence of minor tremor activities without corresponding GPS signatures⁹. Similar events have also been documented for other regions with irregular minor tremors, including southern Cascadia²³, Costa Rica²⁴, and southwest Japan^{25,26}. One possible explanation is that the corresponding slip may be too small to be detected by surface GPS measurements. The installation of borehole strainmeters in the region and/or increasing resolution of GPS analysis may be able to provide more diagnostic constraints.

Previous studies have shown that aseismic slips on the interplate thrust zone at depth may slightly elevate the stress along the locked portion of the interface located up-dip^{7,27-29}, and thereby increase the probability of triggering a large subduction thrust

earthquake³⁰. The wide depth distribution of tremors reported here suggests that detailed modeling incorporating various slip scenarios is needed to properly address the possible effect of ETS events on the occurrence of megathrust earthquakes.

Finally, it can be noted that the extraordinarily high signal-to-noise ratio of the Japanese borehole seismic networks enables the identification of *P* and *S* phases of some relatively large seismic tremors. Using more conventional earthquake location methods, the depths of Japanese tremors are determined to be 25–35 km^{25,26}, a range remarkably consistent with the peak of tremor depths reported here (Figure 3). If ETS events in various regions are associated with similar physical processes, then a wide distribution of tremor depths with a peak in the lower crust can be expected. The resolution of this extended depth range will depend on the accurate locations of not only large but also small tremors.

Supplementary Information accompanies the paper on *Nature's* website (<http://www.nature.com>).

Competing Interests statement The authors declare that they have no competing financial interests.

Correspondence and requests for materials should be addressed to H.K. (e-mail: hkao@nrca.gc.ca).

1. Atwater, B. F. Evidence for great Holocene earthquakes along the outer coast of Washington state. *Science* **236**, 942-944 (1987).
2. Atwater, B. F. & Hemphill-Haley, E. Recurrence intervals for great earthquakes of the past 3500 years at northeastern Willapa Bay, Washington. *U.S. Geol. Surv. Prof. Pap. 1576*, 108 pp. (1997).
3. Satake, K., Wang, K. & Atwater, B. F. Fault slip and seismic moment of the 1700 Cascadia earthquake inferred from Japanese tsunami descriptions. *J. Geophys. Res.* **108**, doi:10.1029/2003JB002521 (2003).

4. Savage, J. C. & Lisowski, M. Strain measurements and the potential for a great subduction earthquake off the coast of Washington. *Science* **252**, 101-103 (1991).
5. Dragert, H. & Hyndman, R. D. Continuous GPS monitoring of elastic strain in the northern Cascadia subduction zone. *Geophys. Res. Lett.* **22**, 755-758 (1995).
6. Wang, K., Wells, R., Mazzotti, S., Hyndman, R. D. & Sagiya, T. A revised dislocation model of interseismic deformation of the Cascadia subduction zone. *J. Geophys. Res.* **108**, 2026, doi:10.1029/2001JB001227 (2003).
7. Dragert, H., Wang, K. & James, T. S. A silent slip event on the deeper Cascadia subduction interface. *Science* **292**, 1525-1528 (2001).
8. Miller, M. M., Melbourne, T., Johnson, D. J. & Sumner, W. Q. Periodic slow earthquakes from the Cascadia subduction zone. *Science* **295**, 2423 (2002).
9. Rogers, G. & Dragert, H. Episodic tremor and slip on the Cascadia subduction zone: The chatter of silent slip. *Science* **300**, 1942-1943 (2003).
10. Kao, H. & Shan, S.-J. The Source-Scanning Algorithm: mapping the distribution of seismic sources in time and space. *Geophys. J. Int.* **157**, 589-594 (2004).
11. Ramachandran, K., Dosso, S. E., Spence, G. D., Hyndman, R. D. & Brocher, T. M. Forearc structure beneath southwestern British Columbia: A three-dimensional tomographic velocity model. *J. Geophys. Res.* **110**, B02303, doi: 10.1029/2004JB003258 (2005).
12. Calvert, A. J. Seismic reflection imaging of two megathrust shear zones in the northern Cascadia subduction zone. *Nature* **428**, 163-167 (2004).
13. Nedimovic, M. R., Hyndman, R. D., Ramachandran, K. & Spence, G. D. Reflection signature of seismic and aseismic slip on the northern Cascadia subduction interface. *Nature* **424**, 416-420 (2003).

14. Calvert, A. J. & Clowes, R. M. Deep, high-amplitude reflections from a major shear zone above the subducting Juan de Fuca plate. *Geology* **18**, 1091-1094 (1990).
15. Hyndman, R. D. Dipping seismic reflectors, electrically conductive zones, and trapped water in the crust over a subducting plate. *J. Geophys. Res.* **93**, 13,391-13,405 (1988).
16. Clowes, R. M. et al. LITHOPROBE-southern Vancouver island: Cenozoic subduction complex imaged by deep seismic reflections. *Can. J. Earth Sci.* **24**, 31-51 (1987).
17. Cassidy, J. F. & Ellis, R. M. S wave velocity structure of the northern Cascadia subduction zone. *J. Geophys. Res.* **98**, 4407-4421 (1993).
18. Peacock, S. M. Fluid processes in subduction zones. *Science* **248**, 329-337 (1990).
19. Wang, K. & Hyndman, R. D. Challenges in defining seismogenic zone using geodetic and structural observations. *EOS Trans. AGU* **85**, Fall Meet. Suppl., Abstract S43D-05 (2004).
20. Adam, J., Klaeschen, D., Kukowski, N. & Flueh, E. Upward delamination of Cascadia Basin sediment infill with landward frontal accretion thrusting caused by rapid glacial age material flux. *Tectonics* **23**, TC3009, doi:10.1029/2002TC001475 (2004).
21. von Huene, R., Ranero, C. R. & Vannucchi, P. Generic model of subduction erosion. *Geology* **32**, 913-916 (2004).
22. Hyndman, R. D., Mazzotti, S., Weichert, D. & Rogers, G. C. Frequency of large crustal earthquakes in Puget Sound-Southern Georgia Strait predicted from geodetic and geological deformation rates. *J. Geophys. Res.* **108**, 2033, doi:10.1029/2001JB001710 (2003).

23. Szeliga, W., Melbourne, T. I., Miller, M. M. & Santillan, V. M. Southern Cascadia episodic slow earthquakes. *Geophys. Res. Lett.* **31**, L16602, doi:10.1029/2004GL020824 (2004).
24. Broan, K. M., DeShon, H., Tryon, M., Dorman, L. & Schwartz, S. Transient fluid pulsing and noise in the Costa Rican subduction zone: Nearly silent slip events? *EOS Trans. AGU* **84**, Fall Meet. Suppl., Abstract T41E-06 (2003).
25. Obara, K. Nonvolcanic deep tremor associated with subduction in southwest Japan. *Science* **296**, 1679-1681 (2002).
26. Katsumata, A. & Kamara, N. Low-frequency continuous tremor around the Moho discontinuity away from volcanoes in the southwest Japan. *Geophys. Res. Lett.* **30**, 1020, doi:10.1029/2002GL015981 (2003).
27. Linde, A. T. & Silver, P. G. Elevation changes and the great 1960 Chilean earthquake: Support for aseismic slip. *Geophys. Res. Lett.* **16**, 1305-1308 (1989).
28. Thatcher, W. Seismic triggering and earthquake prediction. *Nature* **299**, 12-13 (1982).
29. Shimazaki, K. & Nakata, T. Time predictable recurrence model for large earthquakes. *Geophys. Res. Lett.* **7**, 279-282 (1980).
30. Mazzotti, S. & Adams, J. Variability of near-term probability for the next great earthquake on the Cascadia subduction zone. *Bull. Seismol. Soc. Am.* **94**, 1954-1959 (2004).

Acknowledgements We thank I. Al-Khoubbi, T. Christie, T. Claydon, and R. Hall for their efforts in deploying and maintaining the seismic network; A. Bird, T. Mulder, and W. Bentkowski for their assistance in seismic data processing; R. Baldwin for his software support; A. Calvert, R. Hyndman, and K. Wang for stimulating discussion; and POLARIS consortium for providing data from the BC POLARIS array. Most SSA computation is done on the Mercury cluster of the University of Victoria. This work is

supported in part by a USGS NEHRP research grant. Geological Survey of Canada contribution no. xxxxxxxx.

Figure 1 Maps showing the distribution of seismograph stations (upper) and the gradual migration path of seismic tremors (lower). CNSN: Canadian National Seismograph Network; POLARIS: Portable Observatories for Lithospheric Analysis and Research Investigating Seismicity. This tremor sequence began on February 25, 2003 (referred as Day 0). Thus D2 means February 27, 2003 and so on. Each white oval represents one standard deviation (from the geometric center) of the spatial distribution of tremors occurring in the annotated day.

Figure 2 Map and profiles showing two seismic tremors occurring at different locations and depths. Normalized brightness function (br), as determined by Source-Scanning Algorithm (SSA), is displayed in color. Higher br means a better consistency between the source location and the observed arrivals of tremor signals. The large depth difference cannot be an artifact because the predicted arrivals from erroneous depths are inconsistent with the observed seismograms (lower panel). Waveforms are plotted in normalized amplitudes, which are used in br calculation. Station name and the corresponding epicentral distance are marked at the beginning of each trace. Notice that the predicted arrival time difference varies with epicentral distance, thus allowing no trade-off between the depth and the origin time.

Figure 3 Two cross sections showing the spatial distribution of seismic tremors with respect to background seismicity, regional tomography, and strong reflectors identified from seismic reflection surveys. Histograms of tremor numbers at various depths are shown to the right of each cross section. Many

tremors occurred within (or close to) the reflectors where local earthquakes are absent (blowups of S84-1 and S84-2). The symbol size of tremors roughly corresponds to the hypocentral uncertainty. To avoid any distortion from projecting over a large distance, only tremors and earthquakes within 15 km from the location of each cross section are used.

Figure 4 A comparison of frequency spectra between local earthquakes and ETS tremors in northern Cascadia. At frequencies between 1 and 5 Hz, the amplitudes of seismic tremors are comparable to that of $M_L \sim 1.5$ earthquakes. However, the high frequency (>5 Hz) content of tremors is much smaller, even less than that of $M_L = 0.2$ earthquakes. Such a dramatic difference in source spectra suggests distinct physical processes for tremors versus local earthquakes.

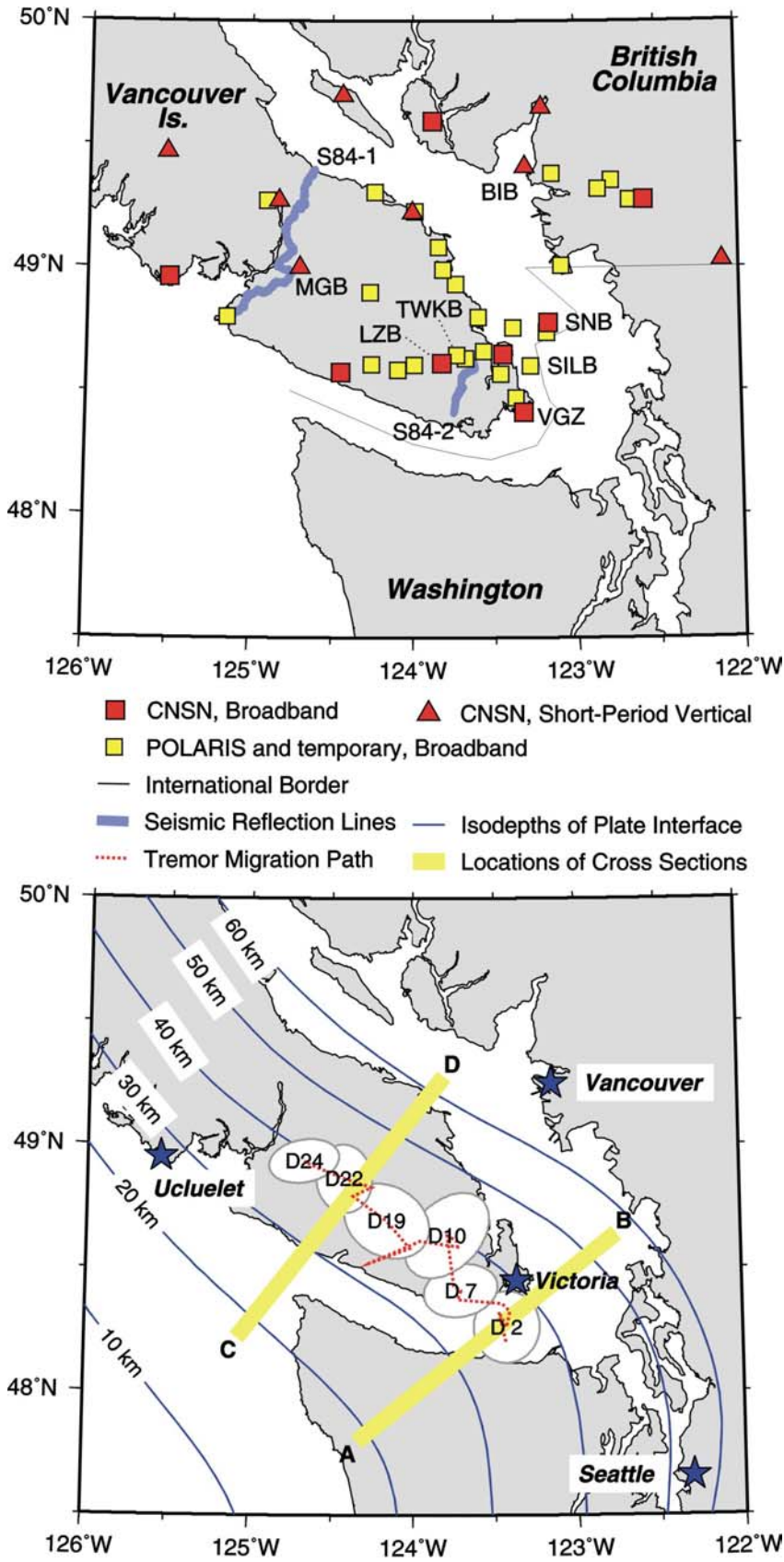


Figure 1

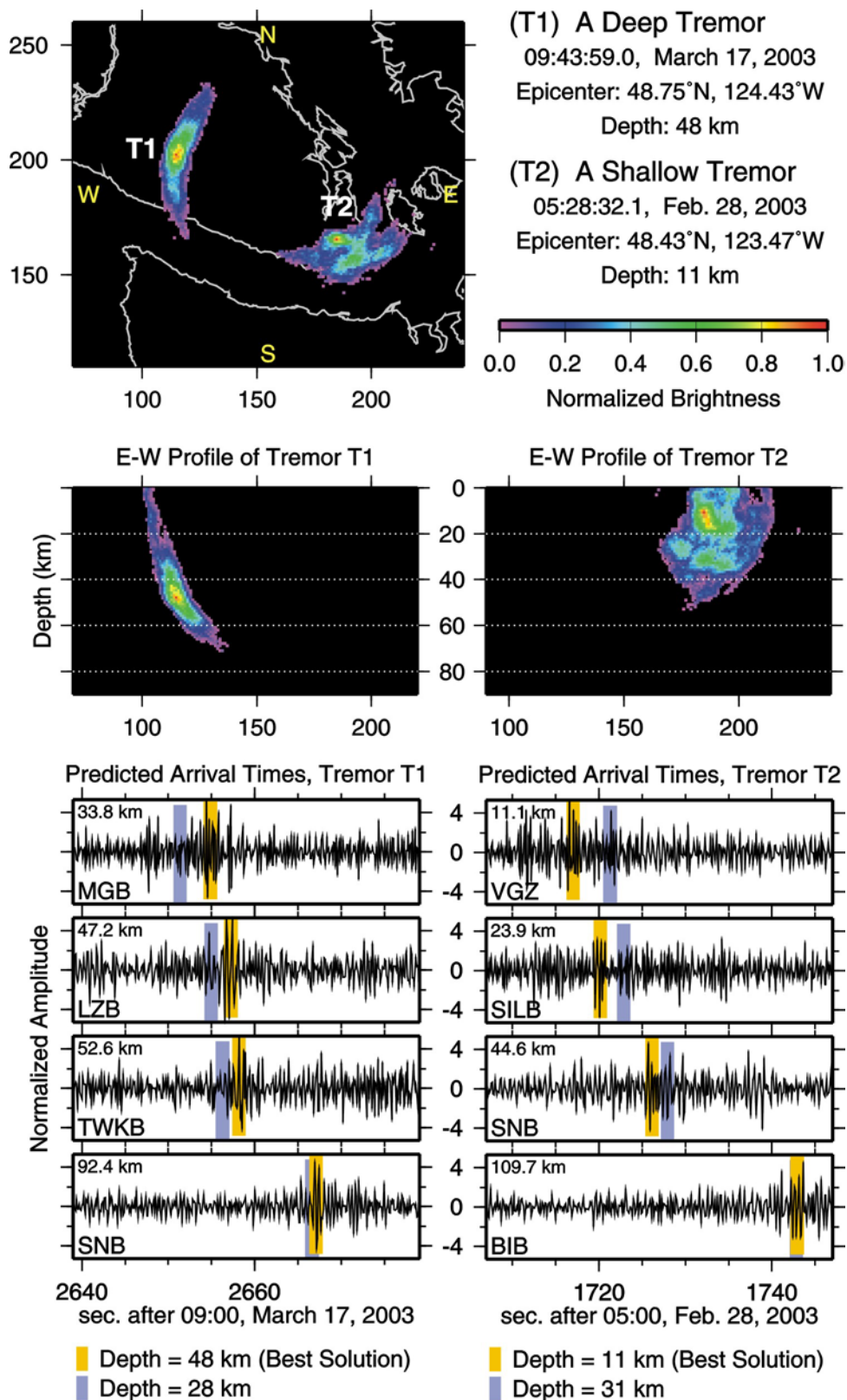


Figure 2

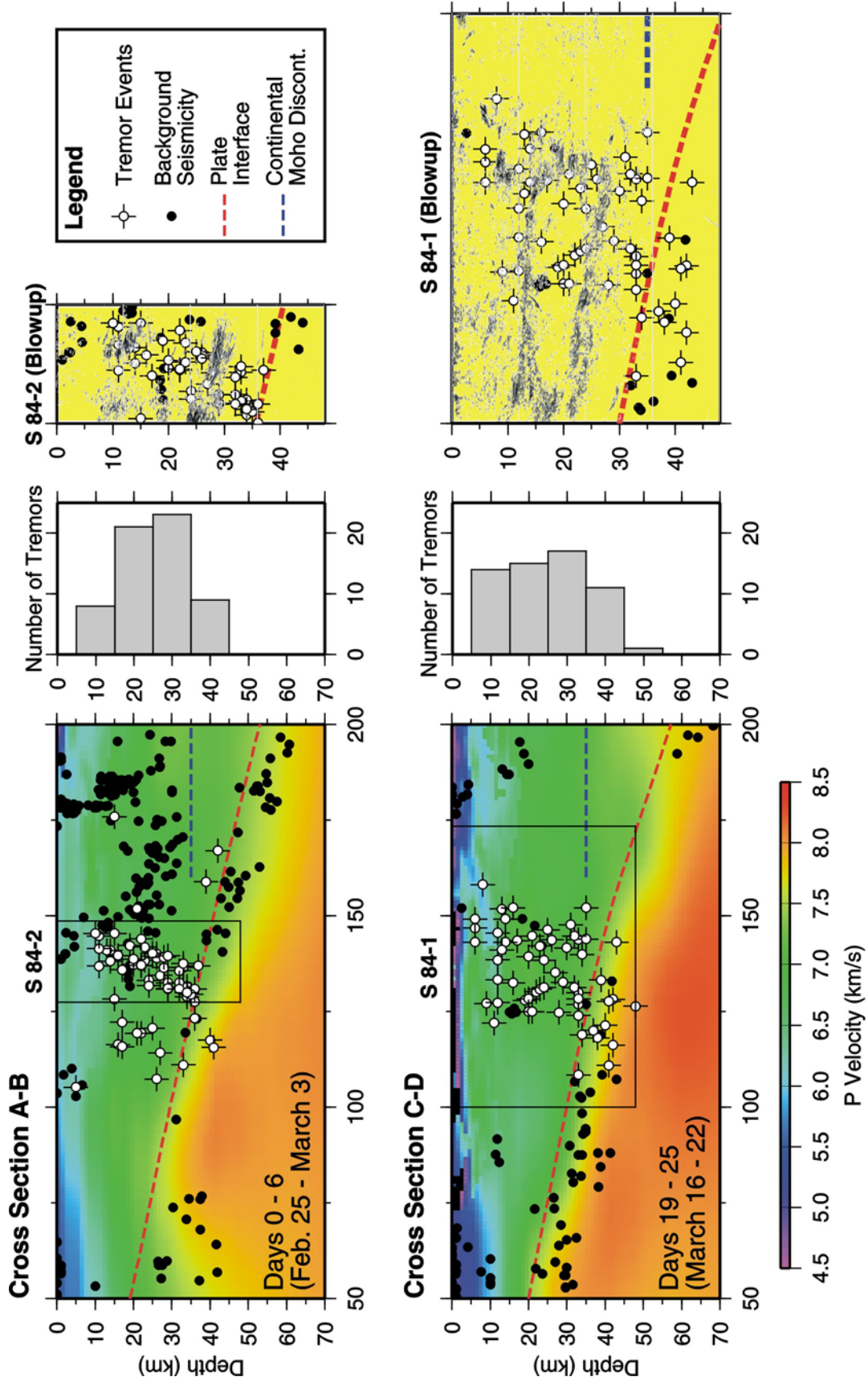
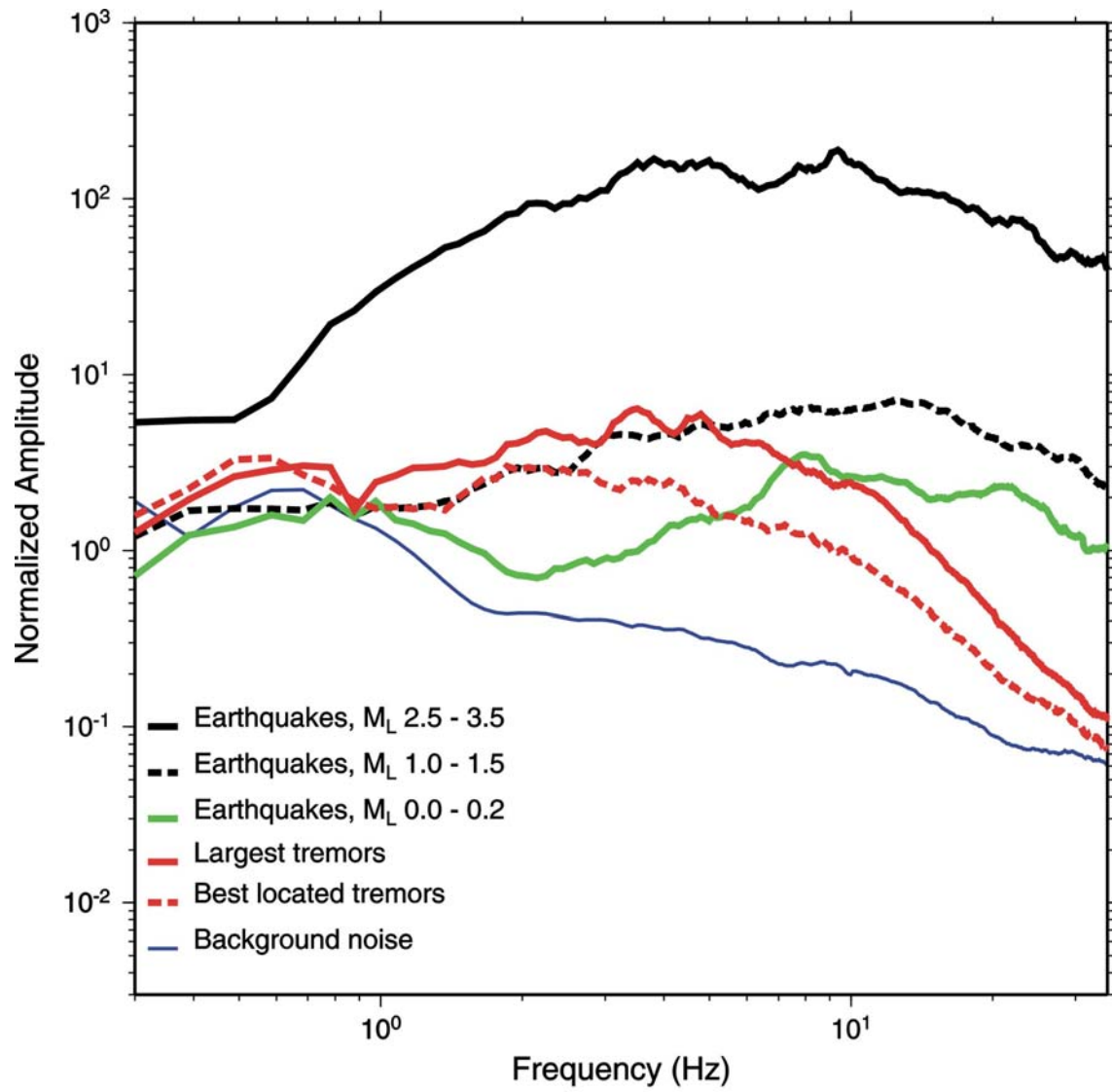


Figure 3

**Figure 4**